Discrete Multi-Tone Transmission with Optimized QAM Constellations for Short-Reach Optical Communications

Siamak Amiralizadeh, Amin Yekani, and Leslie A. Rusch

IEEE/OSA Journal of Lightwave Technology, (Volume 34) (2016)

Doi: 10.1109/JLT.2016.2574598

http://ieeexplore.ieee.org/document/7480764/

This article has been accepted for publication in a future issue of this journal, but has not been fully edited.
Content may change prior to final publication. Citation information: DOI 10.1109/JLT.2016.2574598, Journal of Lightwave Technology.

Discrete Multi-Tone Transmission with Optimized QAM Constellations for Short-Reach Optical Communications

Siamak Amiralizadeh, *Student Member, IEEE,* Amin Yekani, *Student Member, IEEE,* and Leslie A. Rusch, *Fellow, IEEE*

***Abstract*—We investigate performance of optimized M-ary quadrature amplitude modulation (M-QAM) constellations in short-reach single-polarization (SP) and dual-polarization (DP) discrete multi-tone (DMT) with direct detection. The constellations are obtained by using an iterative gradient-search algorithm. For the non-square constellations, we find bit-to-symbol mappings with a blind search method. Our experiments show that data rate can be improved in both SP and DP DMT systems by using optimized constellations instead of square M-QAM. Net data transmission rates of 165 Gb/s and 152 Gb/s are respectively achieved for back-to-back and 2.2 km in a direct-detection DP DMT system assuming forward error correction (FEC) threshold of 3.8×10^{-3}.**

***Index Terms*—Constellations, data center interconnects, direct detection, discrete multi-tone (DMT), optical fiber communication, orthogonal frequency-division multiplexing (OFDM).**

I. Introduction

HIGH capacity short-reach optical communication systems are extensively studied to accommodate bit rate requirements for data centers [1], [2]. Implementation of optical systems with high capacity targets can be demanding in a cost-sensitive scenario. With the recent progress in high-speed digital-to-analog converters (DACs) and analog-to-digital converters (ADCs), intensity modulation with direct detection (IM/DD) can be used to achieve 100 Gb/s and higher data rates per channel at low cost. Several modulation techniques are investigated to accommodate the envisioned data rates in a cost-efficient manner [3]–[8].

Discrete multi-tone (DMT) modulation, a variation of orthogonal frequency-division multiplexing (OFDM), with direct detection is a promising candidate for data centers. DMT is attractive in particular for short-reach optical systems where the optical channel is highly frequency limited due to the use of inexpensive devices (e.g., silicon modulator) and double sideband (DSB) transmission [7]. Optimized bit- and power-loading in DMT maximize data transmission rate for frequency limited components by careful choice of the modulation format and power of each subcarrier for a given signal-to-noise ratio (SNR) per subcarrier [8].

Manuscript received December 01, 2015; accepted May 27, 2016. This work was supported by TELUS and NSERC under CRD grant 437041.

The authors are with the Center for Optics, Photonics, and Lasers (COPL), Electrical and Computer Engineering Department, Université Laval, Québec, QC G1V 0A6, Canada (e-mail: siamak.amiralizadeh-asi.1@ulaval.ca; aminreza.yekani-khoei.1@ulaval.ca; rusch@gel.ulaval.ca).

System capacity can be further improved by expanding the available set of constellations beyond the conventional square quadrature amplitude modulation (QAM), e.g., non-square constellations adapted to the noise characteristics of the channel [9]–[14]. Square QAM constellations are used for their simplicity, but proper choice of non-square geometries improve performance. In OFDM systems, DACs are an essential part of the system; we do not incur extra complexity at the transmitter when exploiting an arbitrary arrangement of the constellation points in in-phase/quadrature (I/Q) plane. At the receiver side, complexity increases due to the requirement for a two-dimensional decision unit with look-up table instead of a conventional QAM slicer [15].

Square QAM constellations with Gray coding offer low bit error rate (BER) to symbol error rate (SER) ratio. For irregular constellations, it is not straightforward (or even possible in most cases) to implement Gray coding. Therefore, non-square constellations can suffer an extra penalty due to bit mapping. It is imperative to identify and employ bit mappings with low BER to SER ratio to retain the improvement obtained in SER.

In this paper, we first explore a short-reach DSB direct-detection DMT system with uniform bit- and power-loading. We will take our learnings from uniform loading and apply them to DMT with optimized bit- and power-loading. For the DMT channel, we use an iterative gradient-search method to generate two sets of optimized M-QAM constellations. Each set contains four constellations, one for each alphabet size (M = 8, 16, 32 and 64) investigated. For the irregular constellations, we find bit-to-symbol mappings that have low SER to BER conversion penalty using a blind search technique. For each constellation size, we investigate SER and BER performance of the three constellation types (standard square QAM and two constellations derived for the channel noise model) in a DMT system with uniform bit and power allocations to all subcarriers. We determine the constellation type offering the best BER performance for each constellation size. Finally, we evaluate BER improvement of the chosen constellations compared to square M-QAM in a direct-detection DMT system with bit- and power-loading. Our experiments study single-polarization (SP) and dual-polarization (DP) systems, both using direct detection. The polarization multiplexing scheme investigated improves spectral efficiency without inducing significant complexity [16], [17].

The paper is organized as follows. In section II, we discuss the noise sources in short-reach DSB direct-detection DMT

This article has been accepted for publication in a future issue of this journal, but has not been fully edited.
Content may change prior to final publication. Citation information: DOI 10.1109/JLT.2016.2574598, Journal of Lightwave Technology.

and identify two channel noise models. In section III, we describe the methodology for finding symbol positions and a bit-to-symbol mapping in the two non-square M-QAM constellation sets, one for each channel model. Section IV is devoted to the DMT experiments. We explain the experimental setup for SP and DP DMT in section IV-A. We present the results for DMT with uniform and optimized loading in section IV-B. Section V concludes the paper.

II. Noise in Short-Reach DMT

Square QAM constellations are not optimal in additive white Gaussian noise (AWGN) [18], but are used for their simplicity. In this section, we discuss under which circumstances direct-detection DMT is an AWGN system, and when a phase rotation (PR) should be taken into account. Understanding the noise distribution motivates our examination of three constellation types. As short-reach systems do not require optical amplification, amplified spontaneous emission (ASE) is not the dominant noise. We describe the noise sources in DMT and the parameters that influence the noise distribution. We use Monte Carlo simulations to explore SNR per subcarrier for various laser linewidths and fiber lengths.

A. Noise Distribution

The optical carrier and the data subcarriers travel at different speeds in optical fiber. This difference during transmission over fiber disturbs their phase coherency, which in turn leads to two noise sources after direct detection: PR and inter-carrier interference (ICI). The PR and ICI arise from the interaction between phase noise (PN) on the laser carrier and chromatic dispersion in fiber in directly detected DMT systems [19]. PR can be approximated by a zero-mean Gaussian random variable influencing the imaginary part of the signal. ICI can be modeled as an additive complex, zero-mean Gaussian random variable. The variance of both PR and ICI increases with increasing laser linewidth and fiber length, or decreasing number of subcarriers. Impairments due to PR become comparable to that of ICI as fiber length increases and number of subcarriers decreases [19]. For short-reach systems, PR is very small compared to ICI.

Ultra-high-speed DACs/ADCs usually suffer from limited bit resolution. Therefore, quantization noise is one of the major impairments in high-capacity DMT systems. High peak-to-average power ratio (PAPR) of the signals exacerbates the undesirable effect of quantization. This quantization noise can be treated as AWGN parameterized by the quantization noise power, which is in turn a function of the number of quantization levels [20].

As we examine short links, we assume small (but non-zero) fixed and deterministic PR and group the Gaussian ICI in the Gaussian receiver and quantization noise. The relative effect of PR and Gaussian noise on the constellations depends on system parameters influencing ICI (laser linewidth, fiber length and fast Fourier transform (FFT) size) and the other Gaussian noise contributions (DAC bit resolution and receiver noise). We expect constellations optimized for AWGN-only and AWGN with small PR to outperform square M-QAM constellations.

B. System Model and Simulations

We evaluate SNR per subcarrier as a function of laser linewidth and fiber length in simulations. Quadrature phase shift keying (QPSK) signaling for all subcarriers is simulated assuming an 8-bit DAC with 64 GS/s sampling rate. The DAC is modeled by a 256-level uniform quantizer along with a 33-GHz fourth-order super-Gaussian low-pass filter [21]. We use FFT size of 1024 and Hermitian symmetry to generate the DSB DMT signal. Eighty subcarriers are left empty in each sideband for oversampling. PN is modeled as a Wiener process. An ideal optical modulator with zero chirp is considered and optical fiber is modeled as a linear medium with dispersion parameter of 17 ps/(nm·km). A thermal noise-limited receiver is assumed with absolute temperature of 300 K, load resistance of 80 Ω, noise-equivalent bandwidth of 64 GHz and responsivity of 0.6. The received power is 0 dBm. A combination of error vector magnitude (EVM) and BER is used to estimate SNR. At low SNR (< 10 dB), BER gives accurate estimation of SNR; however, for high SNRs errors are too few for accurate BER calculation. Therefore, in this regime EVM is more precise for estimating SNR [22].

Fig. 1(a) and Fig. 1(b) show SNR as a function of laser linewidth and subcarrier frequency for 2 km and 10 km fiber lengths, respectively. With 10 km we have significant power fading due to chromatic dispersion inducing disparate delays to the two direct-detected signal sidebands. The linewidth dependence is greatly overshadowed by this effect (note the scale where blue is a deep fade of 25 dB). With 2 km we change the SNR scale to focus on penalty with increased linewidth (blue is a 6 dB penalty). We observe that even when fiber length is as short as 2 km, a laser with large linewidth leads to signal degradation. As an example, with a 2-MHz laser source, SNR is 2 dB and 5 dB lower on average compared to a 100-kHz laser when fiber length is 2 km and 10 km, respectively. Note that results shown in Fig. 1 emphasize performance degradation due to laser PN and fiber chromatic dispersion without discriminating between ICI and PR.

These simulations establish the dominance of PN-induced noise. In the next section, we find the appropriate constellations for short-reach direct-detection DMT. One set of the constellations is optimized for AWGN without any PR and the other set assumes AWGN with small PR.

III. Constellation Design

A. Finding Optimal M-QAM Constellation

QAM constellations optimized for Gaussian noise are derived by minimizing theoretical symbol error probability for a given transmitted power with a gradient-based algorithm [18]. In [23], this method is adopted to optimize the constellations in the presence of both PN and AWGN. Coherent detection is investigated for both weak and strong PN scenarios [11].

We investigate performance of two M-QAM constellation sets when using direct detection. The first one is optimized for AWGN without any rotation of the received symbols; similar to the constellations studied in [18]. The second constellation set is optimized for AWGN with small PR. In the remainder of this paper, the standard square M-QAM,

This article has been accepted for publication in a future issue of this journal, but has not been fully edited.
Content may change prior to final publication. Citation information: DOI 10.1109/JLT.2016.2574598, Journal of Lightwave Technology.

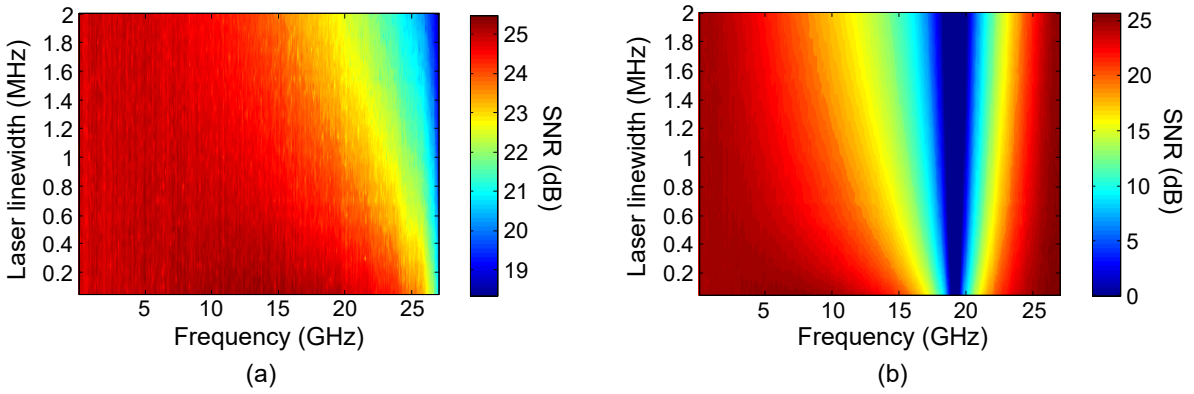

Fig. 1. SNR as a function of laser linewidth and subcarrier frequency for (a) 2 km and (b) 10 km fiber length.

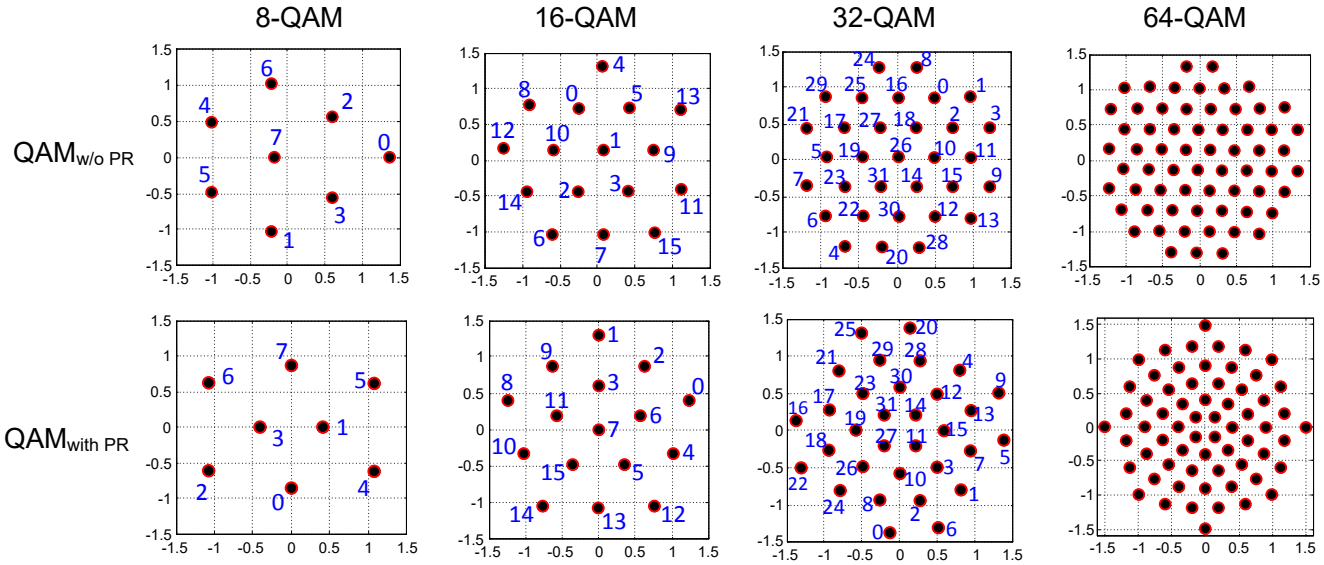

Fig. 2. Two M-QAM constellation sets optimized for short-reach direct-detection DMT. Bit mappings are given in decimal next to the symbol.

the QAM constellations optimized for AWGN without PR and AWGN with PR are respectively referred to as $\mathrm{QAM_{SQ}}$, $\mathrm{QAM_{w/o\,PR}}$ and $\mathrm{QAM_{with\,PR}}$.

In the gradient-search algorithm, four parameters are adjusted to obtain the desired constellation after convergence: Gaussian noise power, step size, initial constellation points and rotation of the transmitted symbols [18], [23]. Gaussian noise power is adjusted to achieve SER of about 4×10^{-3}, close to typical forward error correction (FEC) thresholds. The step size is between 0.01 and 0.001 on the I/Q plane. Square QAM constellation along with several random constellation points serve for initialization. To find $\mathrm{QAM_{with\,PR}}$ constellations, constant rotation of $\pi/18$, $\pi/28$, $\pi/38$ and $\pi/50$ is considered between transmitted and received symbols in 8-, 16-, 32- and 64-QAM, respectively. These angular offset parameters were selected to ensure that the resulting SER is not significantly higher than the AWGN-only case, i.e., the small PR condition. The algorithm converged to the Fig. 2 constellations with less than 5×10^4 iterations.

We note that an exact constellation design requires consideration of all of the system parameters along with their contributions to PR and AWGN. However, it is very difficult (if not impossible) to derive a closed-form solution for SER as a function of all system parameters. The employed approach in finding the constellations and adjusting the parameters of gradient-search algorithm has been proven to provide acceptable accuracy [18], [23]. Furthermore, the gradient-search method is not very sensitive to the Gaussian noise power and the rotation angle when finding the QAM constellations.

B. Bit-to-Symbol Mapping

BER is the ultimate figure of merit, which is dependent on bit-to-symbol mapping for the constellation. $\mathrm{M!}/2$ bit mapping options are available for an M-QAM constellation assuming symmetry between "0" and "1". Testing these options is not feasible for constellations larger than 8-QAM. We adapt the simple blind search technique in [24] minimizing BER, to obtain bit mappings minimizing SER to BER conversion penalty. Let $s_0, ..., s_{M-1}$ denote symbols of constellation set

This article has been accepted for publication in a future issue of this journal, but has not been fully edited.
Content may change prior to final publication. Citation information: DOI 10.1109/JLT.2016.2574598, Journal of Lightwave Technology.

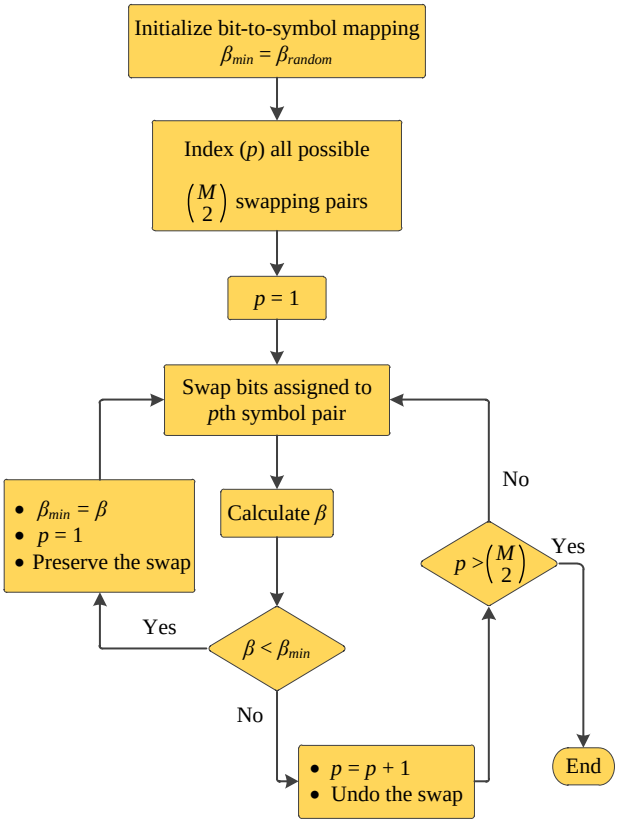

Fig. 3. Flow chart of the bit-to-symbol mapping algorithm. β_{random}: the ratio between BER and SER for the initial random bit mapping.

S with M points on the I/Q plane. The ratio between BER and SER can be approximated as

$$\beta = \frac{\text{BER}}{\text{SER}} \simeq \frac{1}{kM} \sum_{i=0}^{M-1} \bar{H}_i, \tag{1}$$

where $k = \log_2 M$ is the number of bits per symbol and $\bar{H}_i$ is the average Hamming distance between s_i and its neighbouring symbols. Exact calculation would include all constellation points, rather than only neighbouring symbols.

The flow chart shown in Fig. 3 describes the bit mapping algorithm for the non-square QAM constellations. The algorithm starts by randomly assigning bits to all symbols and calculating β per (1). Then a list of all $\binom{M}{2}$ possible swapping pairs for the assigned bits is generated. Beginning by the first pair in the list the bits assigned to the two symbols are switched and β is recalculated. Whenever a lower β is achieved, the algorithm restarts with the new bit mapping and the first pair in the list. The program ends when all of the pairs in the list are tested. The bit mappings found for the non-square constellations are given in Fig. 2.

We also find a lower bound for the estimated β by considering the best bit mapping option for each symbol and its neighbouring symbols, regardless of the bits assigned to the other symbols. For each symbol s_i with n_i neighbouring symbols, we assign "0" (in decimal) to s_i and choose a subset with n_i elements from the set of possible decimal bit mappings

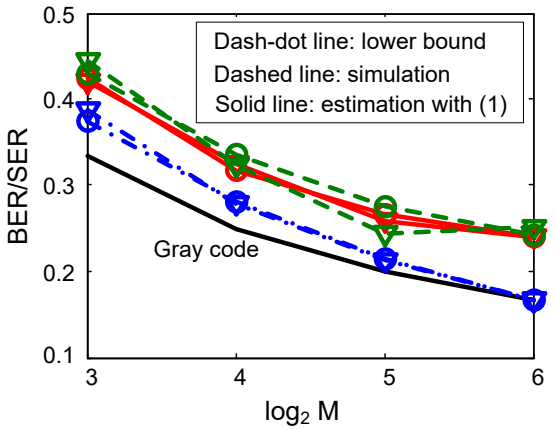

Fig. 4. The ratio between BER and SER versus QAM constellation size. Circles: $\text{QAM}_{\text{w/o PR}}$, triangles: $\text{QAM}_{\text{with PR}}$.

$\{1, 2, ..., M-1\}$ that minimizes $\bar{H}_i$. This gives a lower bound on $\bar{H}_i$, $i = 0, 1, ..., M-1$. We replace these lower bounds in (1) and find a lower bound for β. It is obvious that if $n_i \leq k$, $\bar{H}_{i,LB} = 1$ is the lower bound for average hamming distance between s_i and its neighbouring symbols. If $n_i > k$, the lower bound can be obtained as

$$\bar{H}_{i,LB} = \frac{\sum_{j=1}^{h-1} j\binom{k}{j} + h\left(n_i - \sum_{j=1}^{h-1}\binom{k}{j}\right)}{n_i}, \tag{2}$$

where $h \geq 2$ is an integer satisfying

$$\sum_{j=1}^{h-1}\binom{k}{j} < n_i \leq \sum_{j=1}^{h}\binom{k}{j}. \tag{3}$$

For the constellations studied in this paper, $h = 2$ satisfies (3) since n_i is smaller than or equal to 6. By replacing $h = 2$ in (2), the lower bound simplifies to

$$\bar{H}_{i,LB} = 2 - \frac{k}{n_i}. \tag{4}$$

Therefore, the lower bound for $\bar{H}_i$ can be written as

$$\bar{H}_{i,LB} = \max\left[1, 2 - \frac{k}{n_i}\right]. \tag{5}$$

Replacing $\bar{H}_i$ by $\bar{H}_{i,LB}$ in (1) gives the lower bound for the ratio between BER and SER.

Fig. 4 depicts the ratio between BER and SER for the bit mappings obtained by the blind search algorithm versus QAM constellation size for $\text{QAM}_{\text{w/o PR}}$ (circles) and $\text{QAM}_{\text{with PR}}$ (triangles). In Monte Carlo simulations, we transmit M-QAM OFDM symbols assuming an AWGN channel and direct detection. We find SER and BER by error counting and calculate β. Monte Carlo simulations (dashed lines) show that estimation of β with (1) is relatively accurate for all of the constellations. The obtained bit mappings are close to the lower bound (dash-dot line) for all constellation sizes except 64-QAM. As QAM size increases, the algorithm requires more time to test the bit mappings. Due to the excessive computation time for 64-QAM, it is difficult to investigate a large number

This article has been accepted for publication in a future issue of this journal, but has not been fully edited.
Content may change prior to final publication. Citation information: DOI 10.1109/JLT.2016.2574598, Journal of Lightwave Technology.

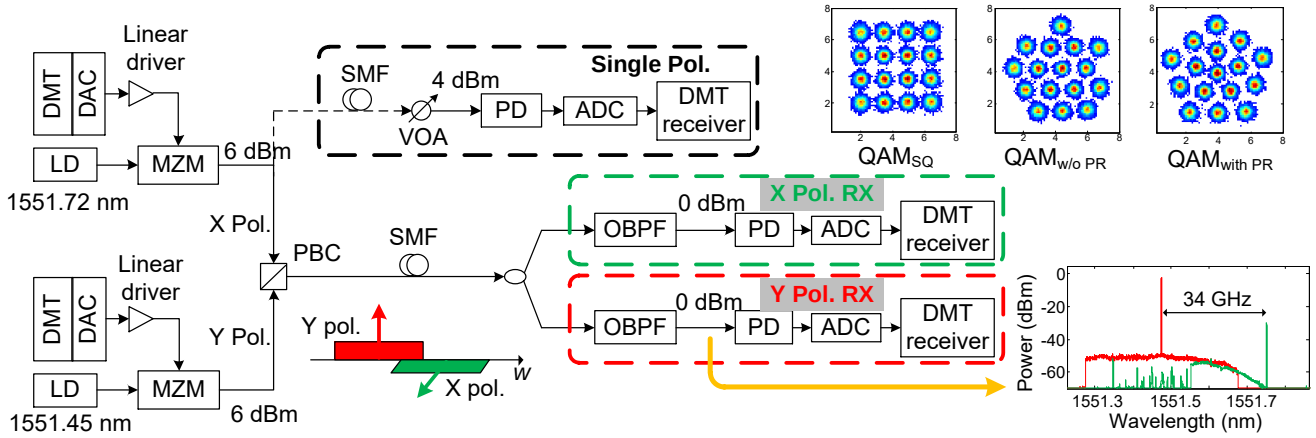

Fig. 5. Experimental setup for SP and DP DSB DMT with direct detection. Insets: sample recovered 16-QAM constellations and signal spectrum at Y polarization receiver. VOA: variable optical attenuator.

of random initial constellations to achieve a bit mapping with low β. We also note that for 8-QAM constellations, all $8!/2$ bit mapping options are tested.

IV. Experimental Assessment

In the experiments, we first examine DMT with a fixed modulation format on all sub-channels to evaluate performance of M-QAM options for different constellation sizes. The performance is measured via both BER and SER. We identify M-QAM constellations offering the best BER performance. Afterwards, we turn to DMT with optimized loading and investigate BER performance of the chosen constellations with minimum BER compared to DMT with $\mathrm{QAM_{SQ}}$.

Spectral efficiency can be increased by employing polarization-division-multiplexing (PDM). Several techniques are used for implementing PDM in direct-detection optical OFDM (DDO-OFDM) [16]. We adopt a simple PDM scheme, originally proposed for single sideband (SSB) DDO-OFDM, which does not require multiple-input multiple-output (MIMO) processing at the receiver but sacrifices spectral efficiency [17]. In this scheme, the carriers for two polarizations are located at different frequencies and the OFDM signal spectra overlap partially. At the receiver for each polarization, an optical band-pass filter (OBPF) is applied to suppress the carrier of the unwanted polarization. In this fashion, each receiver only detects the signal with the same polarization as the surviving carrier. The PDM scheme we use increases spectral efficiency compared to a wavelength-division multiplexing (WDM) system, since it allows partial overlap of the signal spectra. While stability of the OBPF center frequency is critical for SSB OFDM systems, DSB signals are much less sensitive to center frequency offset. We verified in our experiments that even with 6 GHz variation of the OBPF center frequency, BER increase is less than twofold. These features make the employed PDM technique compelling for practical implementation of short-reach PDM DMT.

A. Experimental Setup

Fig. 5 depicts the experimental setup for SP and DP DSB DMT with direct detection. Two independent OFDM signals for X and Y polarization are generated offline by Matlab and converted to analog signals by 64-GS/s DACs with 15 GHz bandwidth and 8 bits resolution. Inverse FFT size is 1024 and eight samples are appended to the time-domain signal as cyclic prefix (CP), which leads to 0.78% overhead. Pre-emphasis is employed to compensate for limited DAC bandwidth only when uniform loading is used. For DMT with optimized loading, we estimate SNR by transmitting QPSK signals with the same power on all subcarriers. We do power and bit allocations based on Chow's margin-adaptive algorithm [25]. The amplified DAC signals drive two $LiNbO_3$ Mach-Zehnder modulators (MZMs) modulating two tones at 1551.72 nm and 1551.45 nm for X and Y polarization, respectively. The MZMs are biased at the quadrature point. The optical carriers are two laser diodes (LDs) with 100 kHz linewidth and 16 dBm output power. The launched power to the fiber is 6 dBm.

For SP DMT, the signals are transmitted over standard single-mode fiber (SMF). The DMT signals with 4 dBm power are detected by a single PIN photodiode (PD). For DP DMT, the signals from MZMs are combined by a polarization beam combiner (PBC) to form a PDM signal and transmitted over SMF. At the receiver for each polarization, an OBPF with 4 dB loss rejects the carrier for the unwanted polarization (22 dB suppression). The received power is 0 dBm for both polarizations. The signals after PD are digitized at 80 GS/s by a 30-GHz real-time oscilloscope (RTO) and processed offline to recover the transmitted data.

At the receiver digital signal processing (DSP) block, we resample the digital signals captured by RTO and do frame synchronization. We remove the CP and perform an FFT to obtain the frequency-domain signal. We use OFDM preamble symbols for channel estimation in frequency domain. The overhead due to training symbols is 7.8%. After channel equalization with a single-tap equalizer, decisions are made on the symbols and SER (or BER) is calculated, detecting at least 100 symbol errors. The signal spectrum at the Y polarization receiver is an inset in Fig 5. The two polarizations are superimposed to highlight the impact of filtering on both polarizations. Sample recovered 16-QAM constellations are shown in the inset of Fig. 5.

This article has been accepted for publication in a future issue of this journal, but has not been fully edited.
Content may change prior to final publication. Citation information: DOI 10.1109/JLT.2016.2574598, Journal of Lightwave Technology.

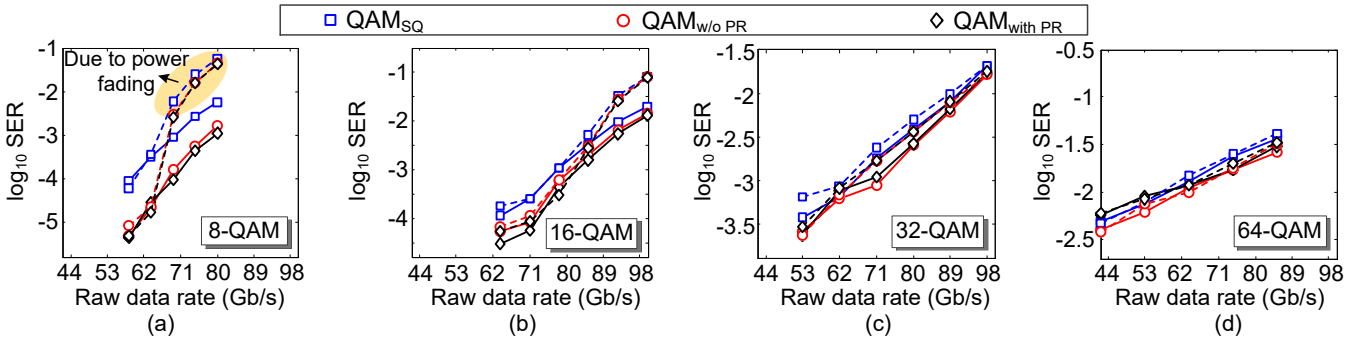

Fig. 6. SER versus raw bit rate for SP DMT with uniform loading with $\mathrm{QAM_{SQ}}$, $\mathrm{QAM_{w/o\,PR}}$ and $\mathrm{QAM_{with\,PR}}$. Solid line: B2B, dashed line: 2.2 km.

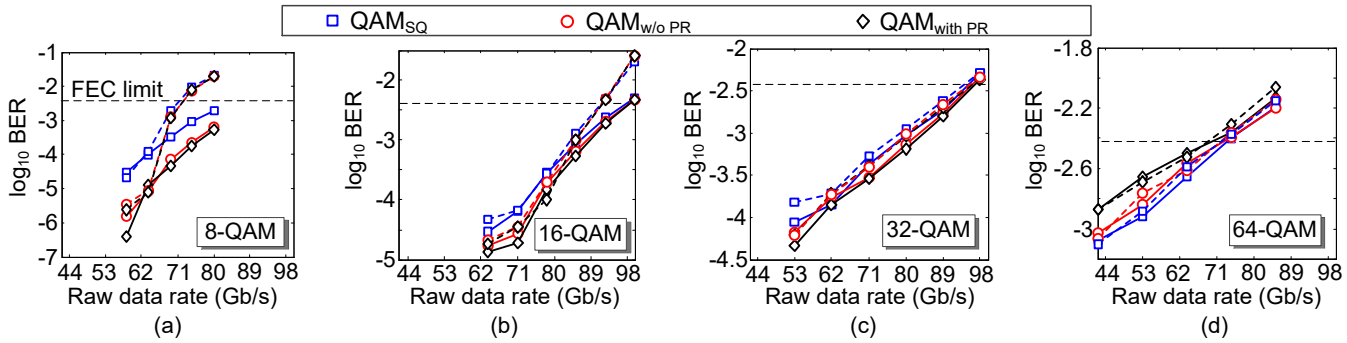

Fig. 7. BER versus raw bit rate for SP DMT with uniform loading with $\mathrm{QAM_{SQ}}$, $\mathrm{QAM_{w/o\,PR}}$ and $\mathrm{QAM_{with\,PR}}$. Solid line: B2B, dashed line: 2.2 km.

B. Results

Fig. 6 shows SER versus raw data rate for SP DMT with uniform loading and different constellation designs for back-to-back (B2B) and 2.2 km transmission. Results for B2B and 2.2 km are shown with solid lines and dashed lines, respectively. SER performance of the optimized constellations is better than that of $\mathrm{QAM_{SQ}}$. The improvement is noticeable for 8-QAM and 16-QAM, whereas 32-QAM and 64-QAM show very small improvement. $\mathrm{QAM_{with\,PR}}$ and $\mathrm{QAM_{w/o\,PR}}$ exhibit similar performance. We also notice the SER degradation due to power fading when signal bandwidth is higher than 25 GHz; see for example the highlighted section of Fig. 6(a) for 8-QAM. Note that in the case of DMT with uniform loading, different data rates are achieved by varying the signal bandwidth.

In Fig. 7, we show measured BER versus raw data rate for SP DMT with uniform bit- and power-loading. BER of 3.8×10^{-3} is assumed for the FEC limit with 7% overhead. The improvement in BER is less pronounced than the SER improvement for the optimized constellations. $\mathrm{QAM_{with\,PR}}$ and $\mathrm{QAM_{w/o\,PR}}$ lose performance compared to $\mathrm{QAM_{SQ}}$ after symbol-to-bit mapping. As discussed in section III-B, the ratio between BER and SER for the optimized constellations is higher than the square QAM constellations with Gray coding. For 8-QAM, the achieved BER improvement is still noticeable. 16-QAM and 32-QAM optimized constellations show very small BER decrease. For 64-QAM, we observe $\mathrm{QAM_{SQ}}$ offers better BER compared to $\mathrm{QAM_{with\,PR}}$ and $\mathrm{QAM_{w/o\,PR}}$.

Average BER of X and Y polarization for 8-QAM and 16-QAM PDM DMT with uniform loading after 2.2 km transmission are shown in Fig. 8. Compared to $\mathrm{QAM_{SQ}}$, using $\mathrm{QAM_{with\,PR}}$ and $\mathrm{QAM_{w/o\,PR}}$ leads to 4 Gb/s and 2 Gb/s data rate increase per polarization for 8-QAM and 16-QAM, respectively. Raw data rate per polarization of 66 Gb/s and 76.5 Gb/s with BER below the FEC threshold is achieved for 8-QAM and 16-QAM, respectively. In the DP DMT, the achieved data rate per polarization is lower than the SP system. In addition to crosstalk between the two polarizations, the difference originates from lower received power to the PD in DP DMT compared to SP DMT (0 dBm versus 4 dBm).

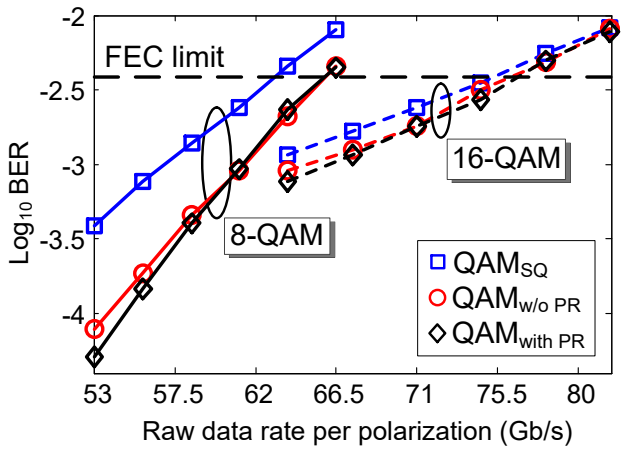

Fig. 8. Average BER for X and Y polarization versus raw data rate per polarization for PDM DMT with uniform loading with $\mathrm{QAM_{SQ}}$, $\mathrm{QAM_{w/o\,PR}}$ and $\mathrm{QAM_{with\,PR}}$ after 2.2 km.

This article has been accepted for publication in a future issue of this journal, but has not been fully edited.
Content may change prior to final publication. Citation information: DOI 10.1109/JLT.2016.2574598, Journal of Lightwave Technology.

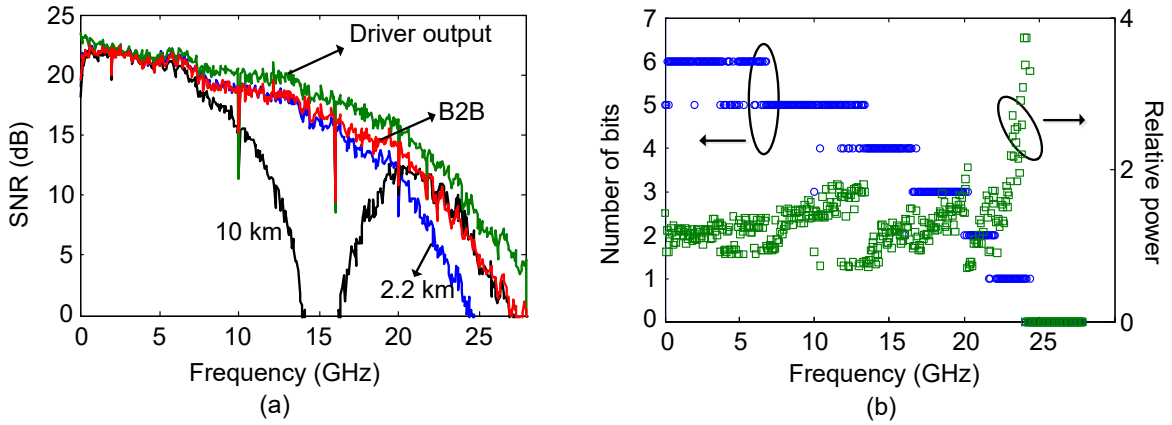

Fig. 9. (a) Measured SNR versus subcarrier frequency. (b) Bit and power allocations for subcarriers when raw data rate is 92.5 Gb/s and fiber length is 2.2 km.

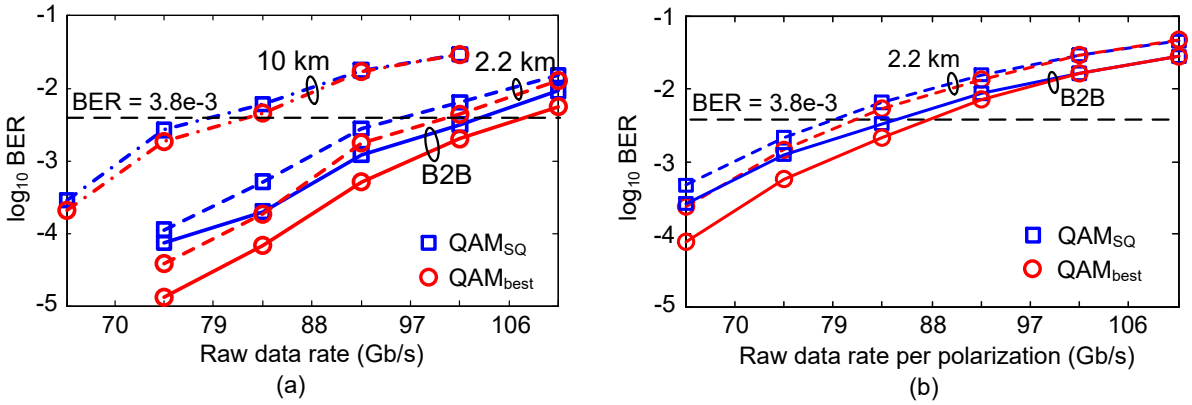

Fig. 10. (a) BER versus raw data rate for SP DMT with optimized loading and with $\mathrm{QAM_{SQ}}$ and $\mathrm{QAM_{best}}$ constellations. (b) Average BER for X and Y polarization versus raw data rate per polarization for DP DMT with optimized loading and with $\mathrm{QAM_{SQ}}$ and $\mathrm{QAM_{best}}$ constellations.

PN-induced ICI and PR are negligible compared to the other noise sources in our experiments since we use a narrow linewidth laser, hence we expected the constellations without PR to work best. In fact, QAM with PR works slightly better, most likely due to a residual PR when applying the single-tap equalizer. When using a wide linewidth laser, PN-induced effects would be stronger, and QAM constellations designed with the assumption of small PR are expected to still work best.

Bit- and power-loading in DMT improve data transmission rate compared to uniform power and bit allocations for optical communication systems that are frequency-limited. Data rate can be further increased by optimizing the constellation shapes used in DMT. We use the QAM constellations leading to minimum BER for each constellation size, as determined in Fig. 7. The best constellation options are: $\mathrm{QAM_{with\,PR}}$ for $\mathrm{M} = 8, 16$ and 32 and standard square for 64-QAM.

In the remainder of this section, we present the experimental results for DMT with optimized bit- and power-loading. We investigate BER performance of the optimized QAM constellations ($\mathrm{QAM_{best}}$) and evaluate the improvement compared to $\mathrm{QAM_{SQ}}$. We also summarize the achieved maximum net data rates with BER below the FEC threshold for different schemes examined throughout this paper.

Fig. 9(a) depicts measured SNR versus frequency for electrical and optical B2B and transmission up to 10 km. Low power of high-frequency subcarriers are due to limited DAC frequency response. Pre-emphasis is not applied as it gives very little data rate improvement for DMT with optimized loading [26]. Fig. 9(b) shows an example of bit and power allocations based on Chow's margin-adaptive algorithm for 92.5 Gb/s SP DMT with 2.2 km transmission. In the DMT with optimized bit- and power-loading, a maximum of 448 subcarriers are used to carry data, which corresponds to 28 GHz electrical DMT signal bandwidth.

Measured BER versus data rate for SP DMT with bit- and power-loading is depicted in Fig. 10(a). DMT with $\mathrm{QAM_{SQ}}$ and $\mathrm{QAM_{best}}$ is shown with squares and circles, respectively. The optimized constellations improve data rate by 4 Gb/s at the FEC threshold. The obtained improvement depends on the bit allocation in DMT. The DMT transmissions with $\mathrm{QAM_{best}}$ and $\mathrm{QAM_{SQ}}$ differ in 8-, 16- and 32-QAM constellations. If more subcarriers use these constellations after bit allocation, the performance improvement will be greater.

Fig. 10(b) shows average X and Y polarization BER versus data rate per polarization for DP DMT with $\mathrm{QAM_{SQ}}$ and $\mathrm{QAM_{best}}$ constellations. Application of optimized QAM constellations leads to consistent data rate increase for B2B and 2.2 km fiber length. Similar to DMT system with uniform loading, in DP DMT the achieved data rate per polarization

TABLE I
NET DATA RATES (GB/S) WITH 7% FEC

	Uniform loading		Optimized loading	
	SP DMT	DP DMT	SP DMT	DP DMT
B2B $\mathrm{QAM_{SQ}}$	91.5	156.5	96.5	159
B2B $\mathrm{QAM_{best}}$	93.5	160	100.5	165
2.2 km $\mathrm{QAM_{SQ}}$	89.5	140.5	90.5	148
2.2 km $\mathrm{QAM_{best}}$	91.5	144	94.5	152

is lower than SP DMT. Our PDs had low receiver sensitivity. Employing a more sensitive PD with transimpedance amplifier (TIA), as it was in the previous demonstrations [6], [7], can alleviate the performance gap between the SP and DP systems.

The net data transmission rates for DMT systems with uniform and optimized loading are summarized in Table I. The total overhead is 15% and includes the overhead due to training symbols for channel estimation, CP and FEC. For B2B system, data rate of 100.5 Gb/s and 165 Gb/s is achieved for SP and DP DMT with optimized loading, respectively. For 2.2 km link, the achieved maximum bit rate is 94.5 Gb/s and 152 Gb/s for SP and DP DMT with optimized loading, respectively. Note that we did not apply error-correcting codes in the experiments. Bit- and power-loading in DMT lead to 5 Gb/s bit rate improvement on average compared to a uniform bit and power allocation. Application of optimized constellations gives 3.6 Gb/s data rate improvement on average compared to square QAM constellations.

V. CONCLUSION

We experimentally demonstrate that performance of SP and DP direct-detection DMT can be improved by using optimized M-QAM constellations. The obtained data rate with BER below the FEC threshold of 3.8×10^{-3} is increased by 6 Gb/s for B2B and 4 Gb/s for 2.2 km span in DP DMT with optimized constellations compared to DMT with square QAM. Application of irregular constellations does not incur extra complexity in the transmitter; it only requires application of a two-dimensional decision unit based on look-up table and modification of the decision boundaries at the receiver. The employed polarization multiplexing scheme is feasible for short-reach applications as its implementation does not require expensive components and MIMO processing.

REFERENCES

[1] Z. Li, I. Shubin, and X. Zhou, "Optical interconnects: recent advances and future challenges," *Opt. Express*, vol. 23, no. 3, pp. 3717–3720, 2015.

[2] J. C. Cartledge and A. S. Karar, "100 Gb/s intensity modulation and direct detection," *J. Lightw. Technol.*, vol. 32, no. 16, pp. 2809–2814, Aug. 2014.

[3] K. Zhong, X. Zhou, T. Gui, L. Tao, Y. Gao, W. Chen, J. Man, L. Zeng, A. P. T. Lau, and C. Lu, "Experimental study of PAM-4, CAP-16, and DMT for 100 Gb/s short reach optical transmission systems," *Opt. Express*, vol. 23, no. 2, pp. 1176–1189, 2015.

[4] X. Xu, E. Zhou, G. N. Liu, T. Zuo, Q. Zhong, L. Zhang, Y. Bao, X. Zhang, J. Li, and Z. Li, "Advanced modulation formats for 400-Gbps short-reach optical inter-connection," *Opt. Express*, vol. 23, no. 1, pp. 492–500, 2015.

[5] K. Zhong, X. Zhou, Y. Gao, W. Chen, J. Man, L. Zeng, A. P. T. Lau, and C. Lu, "140-Gb/s 20-km transmission of PAM-4 signal at 1.3 μm for short reach communications," *IEEE Photon. Technol. Lett.*, vol. 27, no. 16, pp. 1757–1760, Aug. 2015.

[6] Y. Kai, M. Nishihara, T. Tanaka, R. Okabe, T. Takahara, J. C. Rasmussen, H. Ishihara, K. Goi, and K. Ogawa, "130-Gbps DMT transmission using silicon Mach-Zehnder modulator with chirp control at 1.55-μm," presented at the Opt. Fiber Commun. Conf., Los Angeles, CA, USA, 2015, paper Th4A.1.

[7] P. Dong, J. Lee, Y. Chen, L. L. Buhl, S. Chandrasekhar, J. H. Sinsky, and K. Kim, "Four-channel 100-Gb/s per channel discrete multitone modulation using silicon photonic integrated circuits," *J. Lightw. Technol.*, vol. 34, no. 1, pp. 79–84, Jan. 2016.

[8] L. Nadal, M. Svaluto Moreolo, J. M. Fàbrega, A. Dochhan, H. Griesser, M. Eiselt, and J. Elbers, "DMT modulation with adaptive loading for high bit rate transmission over directly detected optical channels," *J. Lightw. Technol.*, vol. 32, no. 21, pp. 4143–4153, Nov. 2014.

[9] S. Amiralizadeh, C. Park, and L. A. Rusch, "Experimental study of M-QAM constellation options for short-reach dual-polarization optical OFDM with direct detection," presented at the Eur. Conf. Opt. Commun., Valencia, Spain, 2015, paper p.4.6.

[10] W. Ling, I. Lyubomirsky, and O. Solgaard, "Digital quadrature amplitude modulation with optimized non-rectangular constellations for 100 Gb/s transmission by a directly-modulated laser," *Opt. Express*, vol. 22, no. 9, pp. 10 844–10 857, 2014.

[11] T. Pfau, X. Liu, and S. Chandrasekhar, "Optimization of 16-ary quadrature amplitude modulation constellations for phase noise impaired channels," presented at the Eur. Conf. Opt. Commun., Geneva, Switzerland, 2011, paper Tu.3.A.6.

[12] T. Pfau, "Noise-resilient constellations for an optical transport system," U.S. Patent 8 693 888, 2014.

[13] L. Beygi, E. Agrell, and M. Karlsson, "Optimization of 16-point ring constellations in the presence of nonlinear phase noise," presented at the Opt. Fiber Commun. Conf., Los Angeles, CA, USA, 2011, paper OThO4.

[14] A. T. Nguyen, W. C. Ng, and L. A. Rusch, "An optimized 16-QAM constellation for mitigating impairments of phase noise and limited transmitter ENOB in optical coherent detection systems," presented at the Eur. Conf. Opt. Commun., Cannes, France, 2014, paper Tu.1.3.5.

[15] B. Guo and C.-M. Hwang, "Multiple payload slicer system with prenormalization integer values," U.S. Patent 6 661 849, 2003.

[16] W. R. Peng, "Direct detection optical OFDM," presented at the Opt. Fiber Commun. Conf., San Francisco, CA, USA, 2014, paper Th3K.7.

[17] A. A. Amin, H. Takahashi, I. Morita, and H. Tanaka, "100-Gb/s direct-detection OFDM transmission on independent polarization tributaries," *IEEE Photon. Technol. Lett.*, vol. 22, no. 7, pp. 468–470, Apr. 2010.

[18] G. J. Foschini, R. Gitlin, and S. Weinstein, "Optimization of two-dimensional signal constellations in the presence of Gaussian noise," *IEEE Trans. Commun.*, vol. 22, no. 1, pp. 28–38, Jan. 1974.

[19] W. R. Peng, "Analysis of laser phase noise effect in direct-detection optical OFDM transmission," *J. Lightw. Technol.*, vol. 28, no. 17, pp. 2526–2536, Sep. 2010.

[20] C. R. Berger, Y. Benlachtar, R. I. Killey, and P. A. Milder, "Theoretical and experimental evaluation of clipping and quantization noise for optical OFDM," *Opt. Express*, vol. 19, no. 18, pp. 17 713–17 728, 2011.

[21] S. Amiralizadeh, A. T. Nguyen, and L. A. Rusch, "Modeling and compensation of transmitter nonlinearity in coherent optical OFDM," *Opt. Express*, vol. 23, no. 20, pp. 26 192–26 207, 2015.

[22] H. A. Mahmoud and H. Arslan, "Error vector magnitude to SNR conversion for nondata-aided receivers," *IEEE Trans. Wireless Commun.*, vol. 8, no. 5, pp. 2694–2704, May 2009.

[23] Y. Li, S. Xu, and H. Yang, "Design of signal constellations in the presence of phase noise," in *Proc. IEEE Vehicular Technology Conference (VTC'08)*, Sep. 2008, pp. 1–5.

[24] D. D. Feldman and F. Chethik, "Two-dimensional constellation generation, pruning, and partial gray coding for bandwidth and power efficiency," U.S. Patent 6 567 477, 2003.

[25] P. S. Chow, J. M. Cioffi, and J. A. C. Bingham, "A practical discrete multitone transceiver loading algorithm for data transmission over spectrally shaped channels," *IEEE Trans. Commun.*, vol. 43, no. 2, pp. 773–775, Apr. 1995.

[26] Z. Liu, T. Richter, C. Schubert, D. J. Richardson, and R. Slavík, "Practical considerations on discrete multi-tone transmission for cost-effective access networks," presented at the Opt. Fiber Commun. Conf., Los Angeles, CA, USA, 2015, paper M3J.4.